NGUYEN DUC HAI

SYNTHESIS OF METAL-ORGANIC FRAMEWORK MODIFIED WITH UiO-66 AND ITS ARSENIC ABSORBING ABILITY IN WATER

Major: Theoretical Chemistry and Physical Chemistry

Code: 9.44.01.19

SUMMARY OF THE DOCTORY OF THEORY CHEMICAL AND CHEMICAL THESIS

Ha Noi – 2023

The work was completed at: Graduate University Science and Technology- Vietnam Academy of Science and Technology.

Science instructor:

1. Assoc.Prof.Dr. Nguyen Dinh Tuyen

2. Assoc.Prof.Dr. Vu Minh Tan

Review 1:

Review 2:

Review 3:

The thesis will be defended in front of the Academy-level PhD Thesis Evaluation Council, meeting at the Graduate University Science and Technology - Vietnam Academy of Science and Technology on ... hour ..., date ... month … years 2023.

Thesis can be found at the library:

- Library of Academy of Science and Technology

- Vietnam National Library

PREAMBLE

1. The urgency of the thesis

The world's clean water resources are declining markedly due to human industrialization activities [1]. Currently, agents such as arsenic (As), dyes, antibiotics, ammonium, heavy metals,... cause serious water pollution [2], [3]. In particular, As is considered one of the most polluting substances in water because it is very toxic, affecting animals and human health even at very low concentrations [4]. People with long-term exposure to arsenic-contaminated water develop cancers of the internal organs including liver, lung and kidney [5]. The World Health Organization (WHO) has set the recommended level for arsenic in drinking water at 10 μg/L. It is estimated that between 94 million and 220 million people are at risk of drinking water with arsenic concentrations >10 μg/L (with 94% of them residing in Asia) [6]. Therefore, As treatment methods are interested and developed by researchers to save costs. Currently, methods to remove As from water sources such as chemical coagulation, reverse osmosis, ion exchange, membrane filtration and adsorption methods [7]. Among the above methods, the adsorption method is highly effective and cost-effective [8]. Some materials used for As adsorption include activated carbon (AC), clay minerals, FexOy, ion exchange resins, etc [9]. However, the adsorption capacity, selectivity, and adsorption rate of these materials are low, so they are not economically viable and practical for application. Recently, Metal–organic framework (MOFs) used to adsorb pollutants in water are popularly studied due to their high surface area, high mechanical stability, and high mechanical stability and the capillary size can be changed appropriately [10]. MOFs are widely applied in fields such as adsorption, catalysis, electro-chemistry, energy storage, photocatalysis, electric battery [11], [12], [13]. Indeed, thanks to their chemical stability, MOFs are used to remove toxic elements from water. Metallic metal–organic framework material containing two metals Co and Fe (Co-Fe-MOF-74) can adsorb As(III) and As(V) at 266.52 and 292.29 mg/g, respectively [14]. The δ-MnO$_2$@Fe/Co-MOF-74, Fe/Mg-MIL-88B materials adsorb As(III) with maximum capacity of 300.5 and 303.6 mg/g, respectively [15], [16]. UiO-66 material with defects, lack of bonds

synthesized by solvent heat method can adsorb up to 303 mg/g As(V) in water. Thus, the mentioned MOFs, UiO-66 showed the highest arsenic absorption compared with other commercial and synthetic adsorbents [9].

The UiO-66 (Zr) material with defects are usually synthesized at high reaction temperature (150-200 $^\circ$C), high pressure, nucleation time, long crystallization (24-96 h), high consumption energy and large particle size (1-10 μm). Therefore, in order to integrate with the new development trend in the world about MOFs, we have chosen the topic "Research to synthesis of metal organic framework material UiO-66 and asen possibility in water environment". In this thesis, I synthesized UiO-66 material containing Zr by solvent heat method and used different modulators (HCl acid, acetic acid and CTABr) to create UiO-66 material with many defects. Then, the UiO-66 material is modified with Fe^{3+} to create more active centers and defects. UiO-66 materials is applied in the research to remove As(V) from the water environment. The influencing factors of pH, initial As(V) concentration, adsorption kinetics and As(V) adsorption mechanism were studied.

2. Research objectives of the thesis

Research and synthesize materials UiO-66, UiO-66 with many defects and applications to remove As(V) in water. Evaluation of As(V) adsorption capacity and study of As(V) kinetics and mechanism.

3. Research content of the thesis

Synthesis of UiO-66 materials with many defects using different modifiers (HCl acid, acetic acid, CTABr).

Characterization of the physicochemical properties, morphology and structure of the synthesized materials by XRD, FT-IR, SEM, TEM, EDX, BET, XPS, TG-DTA methods.

Evaluation of adsorption capacity, removal rate of As(V) and investigation of factors affecting the adsorption process of As(V) such as pH and concentration of As(V).

Kinetic study and proposal of As(V) adsorption mechanism of Fe-UiO-66-CTABr-0,05 material.

4. Layout of thesis

The thesis includes 109 pages, 63 figures, 16 tables and 120 references. The thesis layout includes the following parts: introduction, 3 chapters of content and conclusion. The new contributions of the thesis have been published in 05 prestigious articles in domestic and international scientific journals.

CHAPTER 1. OVERVIEW

Chapter 1 is presented in 40 pages, in which general introduction of MOFs materials, methods of MOFs synthesis, applications of MOFs materials. In the applications of MOFs, the application as an adsorbent is quite new and has not been studied much in Vietnam. From an overview of the research situation on MOFs in the world and in the country, it can be seen that nanostructured MOFs are a new generation of MOFs that are superior to conventional MOFs by special features as small particle size (nm), large pore size (nm), large surface area, large porous volume increases heat transfer, mass transfer, accelerate the diffusion of reactants to the active sites with high dispersion. The research aims to create the lack of bonding defects of UiO-66, in order to increase the physio-chemical and psychoactive properties of the material.

CHAPTER 2. EXPERIENCE

Chapter 2 is presented in 14 pages including:

2.1. Chemicals and equipments

2.2. Experimental process of material synthesis

- The process of synthesizing materials UiO-66
- The process of synthesizing materials UiO-66-Acetic.
- The process of synthesizing materials UiO-66-HCl
- The process of synthesizing materials UiO-66-CTABr
- Synthesis process of Fe-UiO-66-CTABr materials

2.3. Materials characterization methods

Material characterizations determined by modern physical methods, using equipment in Vietnam and UK: XRD, XPS, EDX, SEM, TEM, BET, FT-IR, TGA, UV-Vis.

2.4. Method to evaluate the As(V) adsorption capacity of the synthesized material samples.

- Evaluation of the activity of UiO-66, UiO-66-HCl, UiO-66-Acetic, UiO-66-CTABr, Fe-UiO-66-CTABr materials. Studying the influence of pH, As(V) concentration, reusability of materials,

kinetics and As(V) adsorption mechanism of Fe-UiO-66-CTABr materials.

CHAPTER 3. RESULTS AND DISCUSSION

Chapter 3 is presented in 52 pages including:

3.1. Material characterization results of UiO-66, UiO-66-Acetic, UiO-66-HCl and UiO-66-CTABr samples

3.1.1. XRD results of samples UiO-66, UiO-66-Acetic, UiO-66-HCl and UiO-66-CTABr-0.05 samples
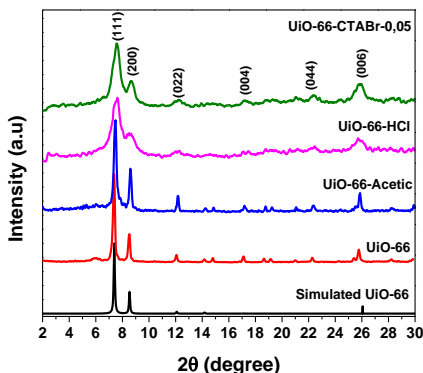
Figure 3.1. XRD patterns of UiO-66, UiO-66-Acetic, UiO-66-HCl and UiO-66-CTABr-0.05 samples

Powder XRD patterns of samples UiO-66, UiO-66-Acetic, UiO-66-HCl and UiO-66-CTABr-0.05 are shown in Figure 3.1. In Figure 3.1, the XRD patterns of UiO-66 sample has peaks at $2\theta \sim 7.2^{\circ}$; 8.3°; 12.0°; 17.0°; 22° and 26° characterize the reflection planes (111), (200), (022), (004), (044) and (006) of UiO-66 phase, respectively [93], [94]. The XRD patterns of UiO-66-Acetic, UiO-66-HCl and UiO-66-CTABr-0.05 samples are similar to that of the standard sample (CCDC No. 733458), which indicates that the UiO-66 sample has been synthesized successfully. Thus, modulators such as HCl, acetic acid, surfactant CTABr do not affect the phase structure of UiO-66. The UiO-66-HCl and UiO-66-CTABr-0.05 samples showed relatively wider and weaker XRD peaks than UiO-66 samples, which indicates that UiO-66 using HCl and CTABr modulators has high resolution low crystallinity and small particle size [95]. In addition,

the presence of HCl also retards the hydrolysis of $ZrOCl_2.8H_2O$ and counteracts the deprotonation of soluble carboxylic acids [66]. Meanwhile, peak intensity of XRD peak of sample UiO-66-Acetic increased compared to sample UiO-66. This shows that the crystallinity of the UiO-66-Acetic sample is significantly increased, due to the fast nucleation and crystallization rates. In addition, acetic acid easily complexed with Zr oxo clusters during the synthesis of MOFs [70].

3.1.2. FT-IR spectra of UiO-66, UiO-66-Acetic, UiO-66-HCl và UiO-66-CTABr-0,05 samples

In FTIR spectra Figure 3.2, fluctuations at 3200 to 3600 cm^{-1} of –OH groups due to adsorbed water molecules inside the capillary [97]. The oscillations at 1583 and 1388 cm^{-1} are assigned to the asymmetric stretching and symmetric stretching of the –COO groups, respectively [93]. The peaks at 746 and 661 cm^{-1} are assigned to the stretching vibrations of Zr−O groups [93], [98].
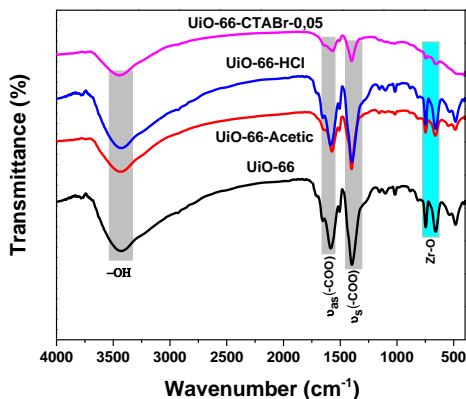
Figure 3.2. FT-IR spectra of UiO-66, UiO-66-Acetic, UiO-66-HCl and UiO-66-CTABr-0,05 samples

3.1.3. SEM and TEM images of UiO-66, UiO-66-Acetic, UiO-66-HCl and UiO-66-CTABr-0,05 samples

The SEM image of UiO-66 sample has a regular, octahedral morphology and the crystals tend to form clusters of large particles about 50-80 nm (Figure 3.3A and Figure 3.4A). The SEM image of

UiO-66-acetic sample shows that the crystals have a grain size of about 100-200 nm, the grain size is not uniform. Thus, the size of UiO-66-acetic sample increased significantly when using the modulator, because acetic acid easily complexed with Zr oxo clusters during the synthesis of MOFs [70]. The reaction yield of UiO-66-acetic sample also increased from 71.6% (UiO-66) to 86.9% (UiO-66-acetic) when using acetic acid as the modulator, due to its high crystallinity and the more regular structure of UiO-66. The SEM image of UiO-66-HCl sample shows that the crystals tend to cluster into large particles of about 0.3-0.5 μm (Figure 3.3C). Thus, the UiO-66 crystals using the HCl modulator have irregular structures, possibly because strong acids have an effect on crystal growth [70].
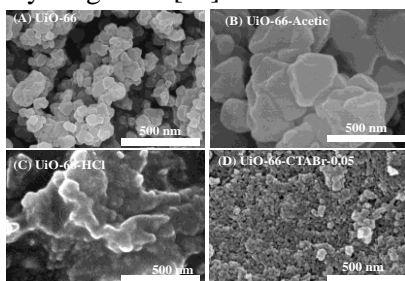
Figure 3.3. SEM images of UiO-66, UiO-66-Acetic, UiO-66-HCl and UiO-66-CTABr-0,05 samples
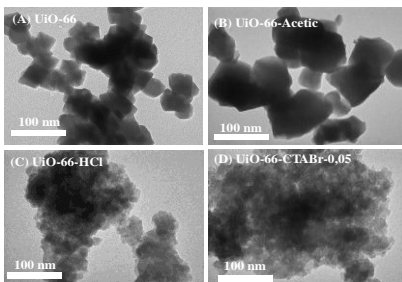
Figure 3.4. TEM images of UiO-66, UiO-66-Acetic, UiO-66-HCl and UiO-66-CTABr-0,05 samples

Table 3.1. Reaction efficiency and particle size of UiO-66, UiO-66-Acetic, UiO-66-HCl and UiO-66-CTABr-0,05 samples

STT	Samples	Modulator	Efficiency (%)	Particle Size (nm)
1	UiO-66	-	71,6	50-80
2	UiO-66-Acetic	Acetic	86,9	100-200
3	UiO-66-HCl	HCl	75,6	20-30
4	UiO-66-CTABr-0,05	CTABr	74,3	20-30

SEM and TEM images of UiO-66-CTABr-0.05 sample (Figure 3.3D and Figure 3.4D) have small particles (20-30 nm), quite uniform due to the enhanced CTABr surfactant high uniformity [100]. This result shows that the presence of surfactant has a good control over the size of the crystals, with a sharp surface [101]. Thus,

the acetic acid modulator can be incorporated into the crystals to partially replace the UiO-66 material binding sequence [66].

3.1.4. N₂ adsorption–desorption isotherms UiO-66, UiO-66 Acetic, UiO-66-HCl and UiO-66-CTABr-0,05 samples
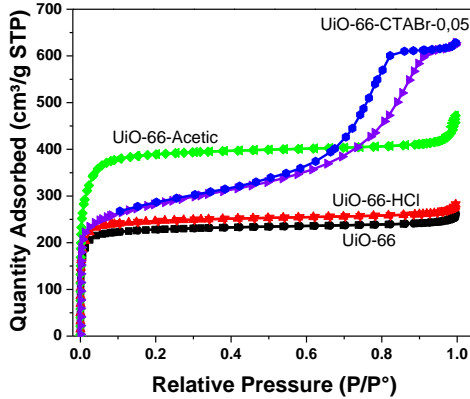
Figure 3.5. N₂ adsorption–desorption isotherms of UiO-66, UiO-66-Acetic, UiO-66-HCl and UiO-66-CTABr-0.05

Table 3.2. Textual characteristics of UiO-66, UiO-66-Acetic, UiO-66-HCl and UiO-66-CTABr-0.05 samples

Samples	S_{BET} (m²/g)	V_{pore}(cm³/g)	D_{BJH} (nm)
UiO-66	939	0,477	2,03
UiO-66-Acetic	1436	0,707	1,66
UiO-66-HCl	974	0,424	1,11
UiO-66-CTABr-0,05	1040	0,962	5,95

In Figure 3.5, the N₂ adsorption–desorption isotherms of UiO-66, UiO-66-Acetic and UiO-66-HCl samples belong to class I according to IUPAC, because mainly microcapillary diameters exist [102]. Meanwhile, the N₂ adsorption-desorption isotherm of UiO-66-CTABr-0.05 sample belongs to class IV, classified according to IUPAC [103]. In Table 3.2, the UiO-66 material has a surface area of 939 m²/g, a pore volume of 0.477 cm³/g and a mean pore diameter (2.03 nm). The UiO-66-Acetic sample has the largest surface area (1436 m²/g), pore volume (0.707 cm³/g) and average pore diameter (1.66 nm). Thus, the UiO-66 sample using acetic acid modulator has

the largest surface area due to the enhanced crystallization of UiO-66 [70]. The UiO-66-HCl sample has a surface area of 974 m^2/g, a pore volume of 0.424 cm^3/g and a mean pore diameter of the smallest (1.11 nm). Meanwhile, the sample UiO-66-CTABr-0.05 has the highest surface area (1040 cm$_2$/g), the largest capillary volume (0.962 cm$_3$/g) and the highest pore diameter (5.95 nm).

3.1.5. Energy Dispersive X-Ray Spectroscopy (EDX) of UiO-66, UiO-66-Acetic, UiO-66-HCl and UiO-66-CTABr-0.05 samples

In Table 3.3, it can be observed that the mass percentage of C and O components in UiO-66-Acetic, UiO-66-HCl and UiO-66-CTABr-0.05 samples decreased compared with UiO-66 sample. In contrast, the contents of Zr in the UiO-66-HCl, UiO-66-Acetic and UiO-66-CTABr-0.05 samples were 30.74, 36.52 and 36.93% mass, respectively. The mass % of C/Zr in UiO-66-Acetic, UiO-66-HCl and UiO-66-CTABr-0.05 was significantly reduced compared with that of UiO-66 sample, due to the formation of many missing structures link [21]. The defect-free UiO-66 (complete structure) is formed by 12 ligands that bridge terephthalate acid with the octahedral cluster $Zr_6O_4(OH)_4$. However, the decrease in the elemental ratio C and C/Zr showed that a $Zr_6O_4(OH)_4$ octahedral cluster could bind with 10 or 8 terephthalate acid bridging ligands (XRD patterns does not show the appearance of ZrO_2 phase) [21].

Total 3.3. Composition % elemental mass of UiO-66, UiO-66-Acetic, UiO-66-HCl và UiO-66-CTABr-0.05 samples

Samples	C	O	Zr	Total	C/Zr
UiO-66	47,60	24,38	28,02	100	1,69
UiO-66-Acetic	41,06	22,42	36,52	100	1,12
UiO-66-HCl	46,49	22,77	30,74	100	1,51
UiO-66-CTABr-0.05	45,52	17,55	36,93	100	1,23

3.1.6. TG-DTA curves of UiO-66, UiO-66-Acetic, UiO-66-HCl and UiO-66-CTABr-0.05 samples

In Figure 3.7A and Table 3.4, the UiO-66, UiO-66-Acetic and UiO-66-CTABr-0.05 samples have 4 stages of mass decline. Specifically, at an early stage the weight loss of about 5-13% at temperatures below 200 °C can be attributed to the removal of physically adsorbed water in the capillaries of the UiO-66 materials.

The subsequent 20-26% weight loss between 200 - 490 °C originates from the removal of chemisorbed water and dehydroxylation of the oxo zirconium clusters in the sample [106].
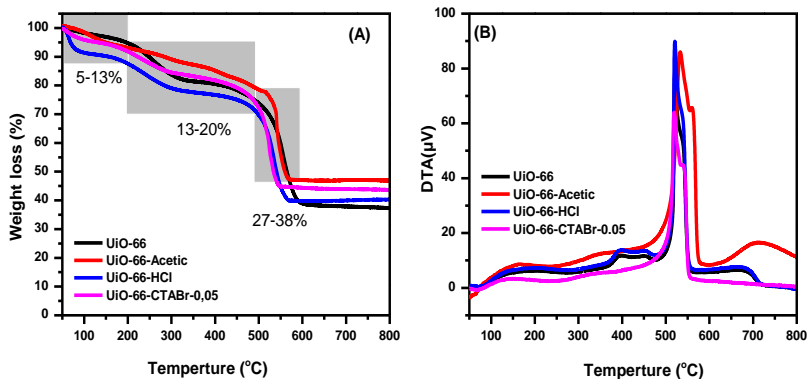
Figure 3.7. TGA curves and (B) DTA of UiO-66, UiO-66-Acetic, UiO-66-HCl and UiO-66-CTABr-0.05 samples

The third stage of weight loss starting at 490 °C is the decomposition of UiO-66 samples due to the combustion of the organically bound molecules in the framework [106]. In the fourth stage, around 600-800 °C, no mass percentage change was observed in all samples, the solid fraction obtained during this period was attributed to the ZrO_2 phase [21]. At the temperature range of 800 ºC, UiO-66, UiO-66-Acetic, UiO-66-HCl and UiO-66-CTABr-0.05 samples have the remaining mass of the samples 37.30%, 46.94%, 40.31% and 43.62%, respectively. Thus, the mass of samples decomposed by heat of UiO-66, UiO-66-Acetic, UiO-66-HCl and UiO-66-CTABr-0.05 samples is 62.70%, 53.06%, 59.69% and 56.38%, respectively. This shows that UiO-66-Acetic and UiO-66-CTABr-0.05 samples have less BDC ligands, which means more binding defects, which is consistent with EDX and XRD results [20]. Figure 3.7B, DTA analysis results show that there is a peak at 520-540 ºC in UiO-66, UiO-66-Acetic, UiO-66-HCl and UiO-66-CTABr-0.05 samples because UiO-66 decomposed and the structure collapsed. In which, the UiO-66-Acetic sample has the highest decomposition temperature (about 540 ºC), which is explained by the UiO-66-Acetic material having the largest particle size (100-200

nm). Meanwhile, UiO-66-CTABr-0.05 sample has the lowest decomposition temperature, this result is explained by the UiO-66-CTABr-0.05 sample with small nanoparticle size (20-30 nm). The TG and DTA results showed that the material samples remained stable up to 490 °C but began to lose the BDC ligand at higher temperatures and decomposed.

3.1.7. XPS spectra of UiO-66, UiO-66-Acetic, UiO-66-HCl and UiO-66-CTABr-0.05 samples
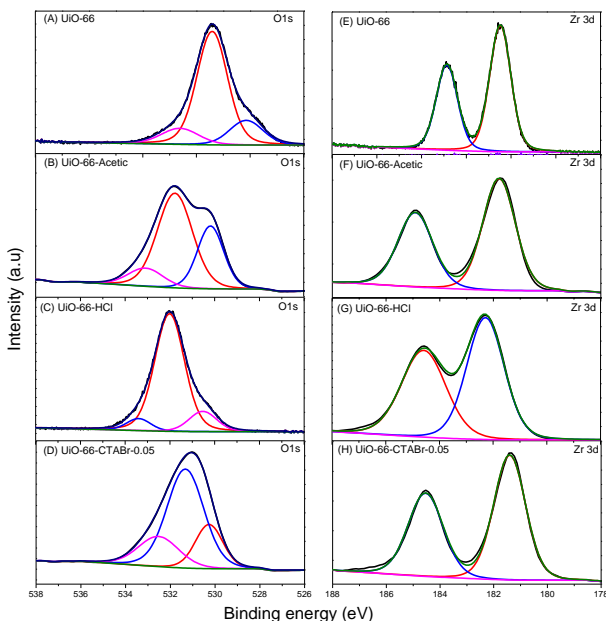
Figure 3.9. High-resolution XPS O 1s spectra of UiO-66 (A), UiO-66-Acetic (B), UiO-66-HCl (C) and UiO-66-CTABr-0.05 (D); High-resolution XPS Zr 3d spectra of UiO-66 (E), UiO-66-Acetic (F), UiO-66-HCl (G) and UiO-66-CTABr-0.05 (H).

The high-resolution O 1s XPS spectra of the UiO-66 sample (Figure 3.9A) shows three peaks at 530.54 eV; 531.99 eV and 533.42 eV can be assigned to oxygen in the metal-bonded lattice (Zr–O), chemisorbed oxygen species, and oxygen in the O–C=O groups [109]. The high-resolution Zr 3d XPS spectra of UiO-66 sample (Figure 3.9E) shows signals at 182.30 and 184.59 eV related to Zr

$3d_{5/2}$ and Zr $3d_{3/2}$, respectively [107]. Thus, the high-resolution O1s and Zr 3d XPS spectra in UiO-66-Acetic, UiO-66-HCl and UiO-66-CTABr-0.05 samples have a shift to a lower binding energy region than with UiO-66 sample, due to partial lack of linkages and the formation of defects in the framework structure [21].

Thus, the UiO-66-CTABr-0.05 nanoparticle size 20-30 nm, capillary diameter (5.95 nm), high surface area was confirmed from the SEM, TEM and BET results. The XRD, EDX and TG-DTA and XPS results show that the UiO-66-CTABr-0.05 sample has an incomplete structure with many defects, which is favorable for the efficient As(V) adsorption process. In summary, the modulator did (i) change the number of nuclei and thus affect the crystal size; and (ii) change in crystallization time affects yield. On that basis, the study used the sample UiO-66-CTABr-0.05 for studies investigating the influence of the ratio of $CTABr/Zr^{4+}$ and denaturation with Fe^{3+}.

3.2. Characteristic results of sample Fe-UiO-66-CTABr-0.05

The UiO-66-CTABr-0.05 sample with nanoparticle size 20-30 nm, surface area 1040 m^2/g, pore volume 0.962 cm^3/g and pore diameter 5.95 nm was used to denature with Fe^{3+}.

3.2.1. X-ray diffraction (XRD) results of Fe-UiO-66-CTABr-0.05 sample
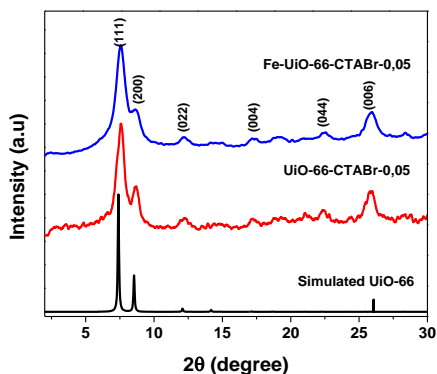
Figure 3.14. XRD patterns of UiO-66-CTABr-0.05 and Fe-UiO-66-CTABr-0.05

In Figure 3.14, the XRD pattern of UiO-66-CTABr-0.05 has peaks at 2θ ~ 7.2º, 8.3º, 12º, 17º, 22º and 26º typical for the reflection

planes (111), (200), (022), (004), (044) and (006) of the UiO-66 phase are similar to the simulation model CCDC No. 733458 [93], [94]. XRD pattern of Fe-UiO-66-CTABr-0.05 sample, after adding Fe^{3+} to UiO-66 structure, no diffraction peaks of α-Fe_2O_3 phase appeared in XRD, because Fe^{3+} was attached onto Zr-oxo clusters in the structure UiO-66-CTABr-0.05 [111]. The characteristic peaks of UiO-66 at $2\theta \sim 7.3^o$, 8.4^o, 12.05^o, 17.1^o, 22.1^o and 26° have a larger shift to 2θ angle than that of UiO-66-CTABr- 0.05 sample, because the Fe^{3+} ion radius (0.64 Å) is smaller than the Zr^{4+} radius (0.82 Å), resulting in a change in the Fe-O (2.15 Å) and Zr-O (2.35 Å) bond lengths [112].

3.2.2. SEM and TEM images of Fe-UiO-66-CTABr-0.05 sample

In Figure 3.16, the UiO-66-CTABr-0.05 and Fe-UiO-66-CTABr-0.05 samples have a particle size of 20-30 nm, the particles are uniform in size and uniformly distributed. Thus, the process of partial replacement of Zr^{4+} by Fe^{3+} on the UiO-66 sample does not affect the morphology and particle size of material. In addition, observing SEM and TEM images of Fe-UiO-66-CTABr-0.05 material, the morphology of the Fe_2O_3 phase was not observed in the sample. The results also show that Fe^{3+} is attached to Zr-oxo clusters in the structure UiO-66-CTABr-0.05 quite uniformly.
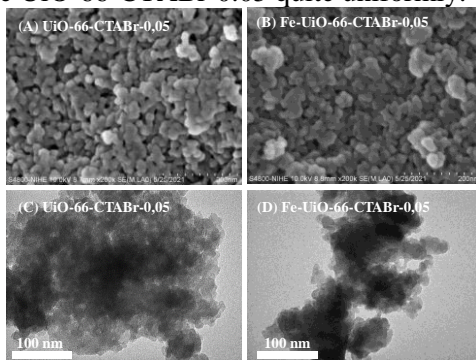
Figure 3.16. SEM and TEM images of UiO-66-CTABr-0.05 and Fe-UiO-66-CTABr-0.05 samples

3.2.3. N₂ adsorption –desorption isotherms of Fe-UiO-66-CTABr-0.05 sample

In Figure 3.17A, the N_2 adsorption –desorption isotherms of all samples belong to class IV, classified according to IUPAC [103]. The UiO-66-CTABr-0.05 material has a large surface area of 1040 m^2/g, a pore volume of 0.962 cm^3/g and the largest mean pore diameter (5.95 nm). For the Fe-UiO-66-CTABr-0.05 sample, the parameters of surface area, pore volume and pore diameter were reduced compared with that of sample UiO-66-CTABr-0.05, due to the bond length Fe-O bond (2.15) smaller than that of Zr-O (2.35) resulting in a shrinking frame structure [112].
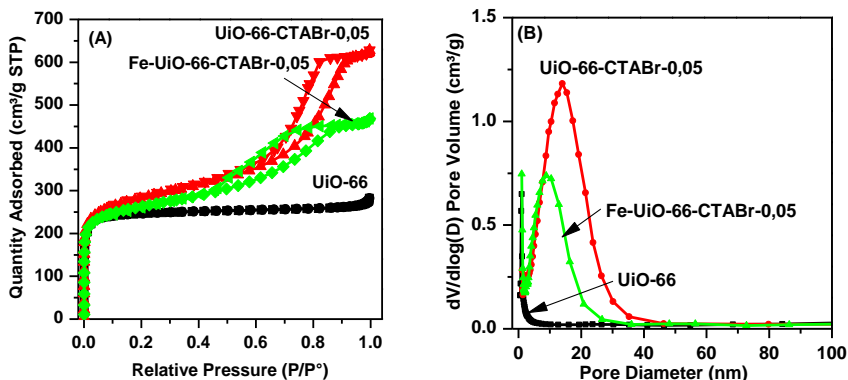
Figure. (A) N_2 adsorption –desorption isotherms and (B) capillary distribution of UiO-66, UiO-66-CTABr-0.05 and Fe-UiO-66-CTABr-0.05 samples

3.2.4. Energy dispersive X-ray (EDX) spectra of Fe-UiO-66-CTABr-0.05 samples

Table 3.7. Elemental mass % composition of UiO-66-CTABr-0.05 and Fe-UiO-66-CTABr-0.05 samples

Samples	C	O	Zr	Fe	Total
UiO-66-CTABr-0.05	45,52	17,55	36,93	-	100
Fe-UiO-66-CTABr-0.05	44,33	18,72	34,00	2,95	100

In Table 3.7, it can be observed that the mass % of C and O components in the Fe-UiO-66-CTABr-0.05 sample decreased compared to that of the UiO-66-CTABr-0.05 sample. In the sample Fe-UiO-66-CTABr-0.05, Fe content accounted for 2.95% by mass,

this result shows that the Fe content in the sample calculated by EDX method is quite close to the Fe content introduced according to the theory. theory (3%).

3.2.5. XPS spectra of UiO-66-CTABr-0.05 and Fe-UiO-66-CTABr-0.05 samples
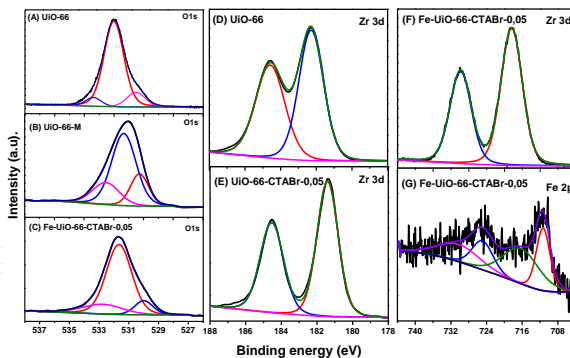
Figure 3.21. High-resolution O1s XPS spectra of UiO-66 (A), UiO-66-CTABr-0.05 (B) and Fe-UiO-66-CTABr-0.05 (C); High-resolution Zr 3d XPS spectra of UiO-66 (D), UiO-66-CTABr-0.05 (E) and Fe-UiO-66-CTABr-0.05 (F); High-resolution Fe 2p XPS spectra of Fe-UiO-66-CTABr-0.05 (G)

The high-resolution O1s XPS spectra of Fe-UiO-66-CTABr-0.05 sample (Figure 3.21C) shows that three peaks at 529.96, 531.66 and 532.84 eV can be assigned to oxygen in metal-bound crystal lattice (Zr–O and Fe-O), chemisorbed oxygen and oxygen in the O–C=O group, respectively [109]. The Zr 3d XPS spectra of Fe-UiO-66-CTABr-0.05 sample (Figure 3.21F) is divided into two peaks at 181.6 and 184.48 eV relative to Zr $3d_{5/2}$ and $3d_{3/2}$, respectively. In the Fe-UiO-66-CTABr-0.05 sample, the peak of Zr $3d_{5/2}$ shifts to a higher binding energy from 181.40 to 181.60 eV due to Fe^{3+} stronger electron attraction than proton, the translation shows Zr-O-Fe bond formation [112]. The Fe 2p XPS spectra of Fe-UiO-66-CTABr-0.05 sample (Figure 3.21G) is divided into four peaks, the binding energies at 711.31 and 724.90 eV are assigned to the existence of Fe^{3+}, binding energies at 716.27 and 730.27 eV are assigned to satellites [114]. The XRD, FTIR and XPS results clearly demonstrated

that Fe^{3+} was attached onto the Zr-oxo clusters via Fe-O-Zr bonding in Fe-UiO-66-CTABr-0.05 [112].

3.3. Evaluation of As(V) adsorption capacity using synthesized materials

3.3.1. Evaluation of As(V) adsorption capacity of UiO-66, UiO-66-Acetic, UiO-66-HCl and UiO-66-CTABr-0.05 samples
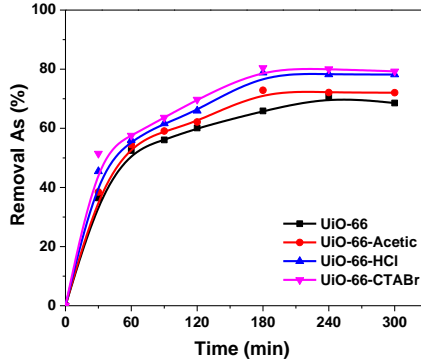
Figure 3.22. As(V) removal capacity of UiO-66, UiO-66-Acetic, UiO-66-HCl and UiO-66-CTABr-0.05 samples

Figure 3.22 shows that UiO-66, UiO-66-Acetic, UiO-66-HCl, UiO-66-CTABr samples have high arsenic adsorption capacity, 70.63, 78.59, 72.57 and 80,26% after 180 minutes of adsorption, respectively. Between 180 and 300 min, the As(V) adsorption efficiency of UiO-66-Acetic, UiO-66-HCl and UiO-66-CTABr-0.05 samples changed insignificantly (slightly decreased). Meanwhile, the UiO-66 sample without defects tends to increase slightly from 70.63 to 71.43% when increasing the adsorption time from 180 to 240 minutes and tends to decrease slightly when increasing the adsorption time 300 minutes. This result shows that the As(V) adsorption rate of UiO-66 samples with defects is faster than that of UiO-66 samples without defects. UiO-66, UiO-66-Acetic, UiO-66-HCl and UiO-66-CTABr samples have high As(V) adsorption efficiency due to the formation of Zr-O-As bonds between UiO-66 and As (V) [18]. According to Wang et al., a cluster of $Zr_6O_4(OH)_4$ at equilibrium can adsorb up to 7 As(V) molecule due to the formation of Zr-O-As bonds, thus the samples UiO-66 and UiO-66 has a defect that can absorb a high amount of As(V) [9].

As(V) adsorption capacity of sample UiO-66-Acetic is higher than that of UiO-66, because sample UiO-66-Acetic has larger pore diameter, capillary volume and specific surface area than UiO-66 sample (Table 3.2), leading to a more favorable process of contact diffusion between the material and As(V). In addition, the defective UiO-66 material samples had a higher percentage of active centers than the non-defective UiO-66 material (Table 3.3). The UiO-66-CTABr-0.05 sample has the highest As(V) removal capacity (80.26%), this is because the UiO-66-CTABr-0.05 material has a large pore diameter (5.95 nm), so it is convenient favorable for As(V) diffusion to the adsorbent surface.

3.3.2. Evaluation of As(V) adsorption capacity of Fe-UiO-66-CTABr-0.05 material

The content of Fe^{3+} in the UiO-66 adsorbent directly affects the removal of As(V). As shown in Figure 3.24, when increasing Fe^{3+} content from 0 to 3%, the removal rate of As(V) of Fe-UiO-66-CTABr-0.05 samples increased significantly, increasing from 80.26 to 94.14 %, which can be explained by the arsenate anion (H_2AsO_4) which can contribute electron pairs to interact with the Fe^{3+} cation (Lewis acid) by acid-base interaction.
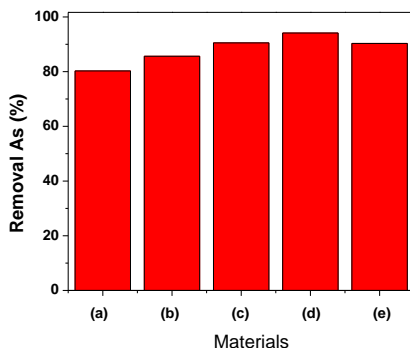
Figure 3.24. Effect of Fe^{3+} content in UiO-66-CTABr-0.05 on the removal rate of As(V)
(a) UiO-66-CTABr-0.05, (b) 1% Fe-UiO-66-CTABr-0.05,
(c) 2% Fe-UiO-66-CTABr-0.05, (d) 3% Fe-UiO-66-CTABr-0.05 and
(e) 4% Fe-UiO-66-CTABr-0.05.

Moreover, the presence of Fe^{3+} ion on the lattice of UiO-66 can create a synergistic effect, increasing the As(V) adsorption efficiency of the material. However, when increasing the Fe^{3+} content from 3 to 4% by mass, the As(V) removal efficiency of the Fe-UiO-66-CTABr sample decreased significantly. Specifically, the removal rate of As(V) decreased from 94.14% to 90.32%, this may be due to the Fe^{3+} content in the sample UiO-66 as shielding and clustering reduces the active sites of materials, so the As(V) removal rate is significantly reduced. The time to reach As(V) adsorption equilibrium of the samples was 180 minutes, so we used Fe-UiO-66-CTABr-0.05 material to investigate the effects of pH on the ratio. remove As(V) for 180 minutes.

3.3.3. Effects of factors on As(V) adsorption of Fe-UiO-66-CTABr-0.05 material

In Figure 3.26A, the pH values directly affect the As(V) removal rate of the Fe-UiO-66-CTABr-0.05 sample. The As(V) removal rate of the Fe-UiO-66-CTABr-0.05 sample increased from 54.5% to 94.06% when the pH values decreased from 11 to 3 (Figure 3.26A). Specifically, at pH in the range 1–5.9, there is an electrostatic interaction between negatively charged As(V) and positively charged adsorbent surface, thus increasing As(V) removal efficiency. In contrast, pH in the range of 5.9-11, the catalyst surface turns negative charge, hinders the interaction and contact between reactants, so the removal rate of As(V) decreases significantly [115].
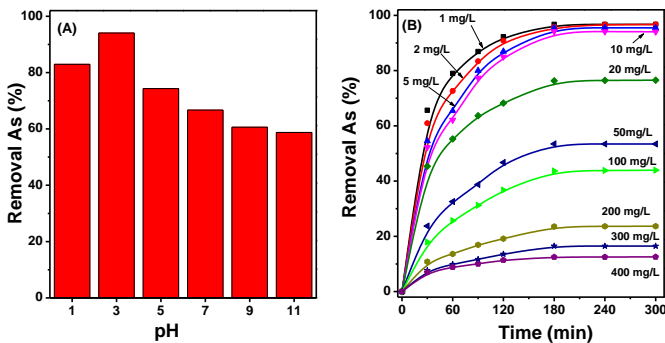
Figure 3.26. (A) The effect of pH value and (B) different As(V) concentrations of Fe-UiO-66-CTABr-0.05.

(adsorption conditions: 0.15 g/L, C_o = 10 mg/L, 3 h, and 25 °C)

At pH = 1, the surface of the adsorbent carries a positive charge, but at low pH (high acidity), the sample Fe-UiO-66-CTABr-0.05 is less stable, so the sample structure is affected influence, so that part of the sample structure is broken, reducing the surface area of the material [116]. In addition, at pH value = 1, As(V) exists in an uncharged state, reducing the interaction of the adsorbent and As(V), leading to a reduced As(V) adsorption rate.

3.3.4. Adsorption isotherm of As(V) onto Fe-UiO-66-CTABr-0.05
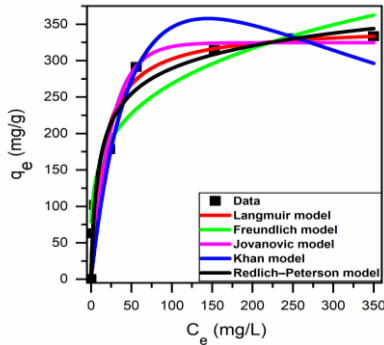
Figure 3.29. Adsorption isotherm of As(V) onto Fe-UiO-66-CTABr-0.05

(adsorption conditions: 0.15 g/L, Co = 10-400 mg/L, 5 h, and 25 °C)

Table 3.11. Isotherm adsorption parameters for As(V) of Fe-UiO-66-CTABr-0.05 sample

Unit	Q_{max} (mg/g)	Parameters of the adsorption models	R^2
Langmuir model	337	R_L =0,067 L/g	0,998
Freundlich model	-	K_F = 0,240 $(mg/g)/(mg/L)^n$	0,9648
Jovanovic model	324	0,041	0,948
Khan model	430	0,007 L/mg	0,889
Redlich–Peterson model	-	0,41 L/g	0,957

The As(V) adsorption capacity of the Fe-UiO-66-CTABr-0.05 sample increased as the As(V) concentration raised to the equilibrium at 333 ppm. The squared regression values of the five As(V) adsorption models are presented in Table 11. The Langmuir model adsorption isotherms are in

good suitable with the test data on equilibrium adsorption compared with such Freundlich, Jovanovic, Redlich–Peterson and Khan models. As(V) adsorption capacity of Fe-UiO-66-M material is about 337 mg/g at pH of 3 and temperature of 25 °C according to the Langmuir model. Therefore, the parameter Q_{max} according to the Langmuir model, is more suitable for the experimental data, so the parameter Q_{max} is used for discussion and comparison. Xingyu et al. [9] synthesized sample UiO-66 by solvent heat method and As(V) adsorption capacity reached 303 mg/g. Gu et al. [16] produced Fe/Mg-MIL-88B material with As(V) adsorption capacity of 303.6 mg/g. In this study, the As(V) adsorption capacity of Fe-UiO-66-CTABr-0.05 sample was 337 mg/g, higher than some previously published MOFs. Therefore, it can be concluded that Fe-UiO-66-CTABr-0.05 is a promising material for the treatment of arsenic contaminated water.

3.3.5. Evaluation reusability of Fe-UiO-66-CTABr-0.05 adsorbent

The removal rate of As(V) on Fe-UiO-66-CTABr-0.05 adsorbent after 4 times of material regeneration is presented in Figure 3.31. Figure 3.31 shows that Fe-UiO-66-CTABr-0.05 material adsorbed As(V) after 4 high reaction cycles, reaching over 80%. This result shows that the Fe-UiO-66-CTABr-0.05 adsorbent has high stability and is stable in the adsorption medium.
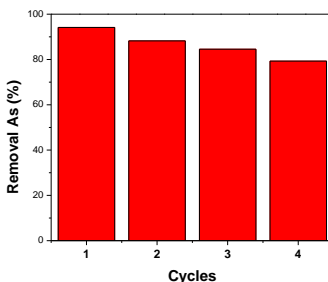
Figure 3.31. As(V) removal rate of Fe-UiO-66-CTABr-0.05 adsorbent after 4 times of material regeneration

XRD methods and SEM images were performed to determine the stability of the Fe-UiO-66-CTABr-0.05 adsorbent. In Figure 3.33, the SEM image of Fe-UiO-66-CTABr-0.05 material after 4 times of material regeneration, the shape and grain size of the material did not change significantly. From the results of the assessment of As(V)

removal ability and characteristic methods such as XRD, SEM, the Fe-UiO-66-CTABr-0.05 material is stable and stable after 4 adsorption cycles.
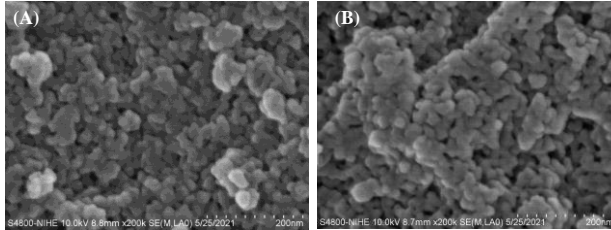
Figure 3.33. SEM image of sample Fe-UiO-66-CTABr-0.05 before (A) and after 4 reaction cycles (B)

3.4. Kinetics and proposed mechanism of As(V) adsorption on Fe-UiO-66-CTABr-0.05 adsorbent

3.4.1. As(V) adsorption kinetics of Fe-UiO-66-CTABr-0.05 . adsorbent

Table 3.14. The correlation coefficient (R^2) of kinetic equations for As(V) uptake by Fe-UiO-66-CTABr-0.05

Kinetic Models	Pseudo-first-order model (R^2)	Pseudo-second-order model (R^2)
Concentration As(V)		
10 mg/L	0.983	0.989
20 mg/L	0.982	0.995
50 mg/L	0.989	0.990
100 mg/L	0.982	0.991
200 mg/L	0.980	0.985
300 mg/L	0.980	0.985
400 mg/L	0.984	0.993

To study As(V) adsorption kinetics of Fe-UiO-66-CTABr-0.05 sample, we assume As(V) adsorption kinetics according to pseudo-first and quadratic models. Information regarding the non-linear forms of pseudo-first and quadratic models is given in Table 3.14. On the basis of statistics (R^2), the pseudo-quadratic model describes the experimental data of the time-dependent adsorption better than the pseudo-first-order model. The obtained results indicate that the kinetics of the adsorption follows the pseudo-second order model. This implies that the chemisorption is very

strong and that As is highly adsorbed on the surface of the Fe-UiO-66-CTABr-0.05 material.

3.4.2. Proposing the As(V) adsorption mechanism of Fe-UiO-66-CTABr-0.05 sample

In Figure 3.35, the FTIR spectra of the sample Fe-UiO-66-CTABr-0.05 before and after As(V) adsorption has a significant change. Specifically, the oscillations at wave numbers 820 cm-1 and 865 cm-1 are assigned to the vibrations of the Fe–O–As, Zr-O-As [117], [118] and As-O groups, respectively. [9], [119]. In addition, there is a high-intensity oscillation at 1688 cm-1 which is attributed to the asymmetric vibration of the As-OH group [119]. The formation of the Zr-O-As coordination is accomplished through electrostatic attraction between the negatively charged As–OH and the positively charged Zr–OH [119]. The formation of the Zr-O-As coordination is accomplished through electrostatic attraction between the negatively charged As–OH and the positively charged Zr–OH [115]. These results demonstrated the formation of complexes between arsenic and the Fe-UiO-66-CTABr-0.05 lattice framework through the formation of a Zr-O-As coordination bond.
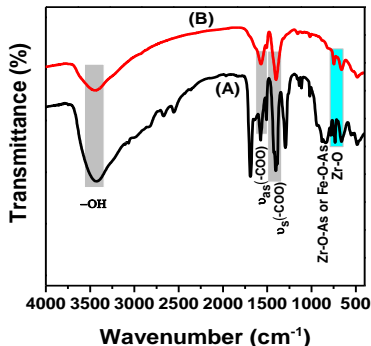
Figure 3.35. FT-IR spectra of Fe-UiO-66-CTABr-0.05 before (A) and after (B) adsorption of As(V)

As shown in Figure 3.36A, the arsenate species (H_3AsO_4) act as the acid binder with the hydroxyl groups in the Zr-containing clusters, then the H^+ ions and the hydroxyl group are released to form water to maintain the balance. by electric charge. In addition, other adsorption sites can exist in the UiO-66 framework by exchanging some BDC ligands with arsenate as shown in Figure 3.36B. Thus, the

molar ratio of Zr:As in the UiO-66 adsorbent is about 6:7 (6 Zr is a cluster of Zr6 that can bind to 7 As) [9].

(A)

$$Zr_6O_4(OH)_4 + n\ H_3AsO_4 \rightarrow Zr_6O_4(OH)_{4-n}(H_2AsO_4)_n + n\ H_2O;\ n \leq 4$$

(B)

$$Zr_6O_4(OH)_4\text{-}OOC\text{-}BDC + H_3AsO_4 \rightarrow Zr_6O_4(OH)_4\text{-}H_2AsO_4 + HOOC\text{-}BDC$$
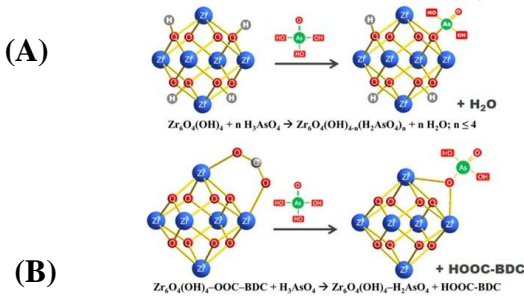
Figure 3.36. As(V) adsorption mechanism of Fe-UiO-66-CTABr-0.05 . material [9]

The exchange of hydroxyl and BDC ligands leads to the formation of complexes between arsenic in the UiO-66 framework. The above coordination processes do not degrade the main crystal structure of the UiO-66 adsorbent. Moreover, at pH < 5.9, Fe-UiO-66-CTABr-0.05 material has a positive charge and As(V) exists in the compound $H_2AsO_4^-$ (negative charge); compound $H_2AsO_4^-$ will ligand anionic and contribute an electron pair that strongly interacts with the central cation Fe3+ (Lewis acid) in the material by acid-base interaction (Figure 3.37). Furthermore, there is an electrostatic interaction between the $H_2AsO_4^-$ anion and the central Fe^{3+} cation in the lattice framework [120].
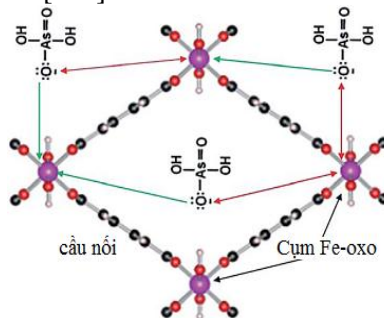
Figure 3.37. Schematic diagram of As(V) adsorption mechanism on Fe-UiO-66-CTABr-0.05 material by electrostatic interaction and Lewis acid-base [120]

CONCLUDE

From the research results of the thesis, we draw the following conclusions:

1) Successfully synthesized UiO-66 materials by solvent heat method using different defect structure modulators (HCl, acetic acid and CTABr). The flawed UiO-66 materials has high surface area (UiO-66-Acetic: 1436 m^2/g), small particle size (20-30 nm) and large capillary diameter (5.95 nm). The Zr content in UiO-66-HCl, UiO-66-Acetic and UiO-66-CTABr materials compared with defect-free UiO-66 materials increased from 28.02 to 36.93% and the ratio C/Zr dropped from 1.69 to 1.12 (EDX result). Similarly, the ZrO_2 content obtained by the TG-DTA method in the UiO-66 samples with many defects (46.94%) was higher than that in the UiO-66 samples without defects (37.30%). The UiO-66, UiO-66-Acetic, UiO-66-HCl and UiO-66-CTABr materials are stable at 490 °C and have the ability to remove As(V) reaching 70.63, 78.59, 72.57 and 80.26% after 180 minutes of As(V) adsorption at the concentration of 10 mg/L, respectively.

2) Modified UiO-66 material with medium capillary structure with Fe^{3+} in the frame structure of UiO-66 (Fe-UiO-66-CTABr-0.05). The Fe-UiO-66-CTABr-0.05 material has a high surface area (980 m^2/g), a particle size of 20-30 nm and stable at 490 °C. The Fe-UiO-66-CTABr-0.05 material is able to remove 94.14% As(V) at the concentration of 10 mg/L and the maximum adsorption capacity reached 337 mg/g at the optimum pH (pH=3). The high As(V) adsorption capacity of the Fe-UiO-66-CTABr-0.05 sample (337 mg/g) due to the formation of a lack of bonding defect in the UiO-66 structure increased the static interaction electricity and the formation of Zr-O-As(V) and Fe-O-As(V) bonds during adsorption.

3) The initial pH value and As(V) concentration affect the As(V) adsorption process. Specifically, pH affects the charge process of Fe-UiO-66-CTABr-0.05 material (pH < 5.9 positively charged materials; vice versa, pH > 5.9 charged materials). The adsorption kinetics data shows that the As(V) adsorption isotherm is consistent with the Langmuir model and follows the pseudo-second-order kinetics equation.

NEW POINT OF THE THESIS

1) Successfully synthesized UiO-66 materials with many defects by using structural modulators HCl, acetic acid and CTABr by solvent heat method and the optimal $CTABr/Zr^{4+}$ ratio was determined to be 0.05. Successfully modified the UiO-66-CTABr-0.05 material with Fe^{3+} in the frame structure UiO-66 (Fe-UiO-66-CTABr-0.05). The post-modified material has a high surface area (980 m^2/g), the particle size is in the range of 20-30 nm and stable at 490 ℃.

2) Initially tested the As(V) adsorption capacity in aqueous solution of the synthesized materials. The results show that the Fe-UiO-66-CTABr-0.05 material can remove 94.14% As(V) at the concentration of 10 mg/L and the maximum adsorption capacity is 337 mg/g at optimal pH (pH = 3). The adsorption on this material follows the second-order apparent adsorption kinetics and the Langmuir adsorption isotherm model.

LIST OF WORKS RELATED TO THE THESIS

1. **Nguyen Duc Hai**, Manh B. Nguyen,Vu Minh Tan, Nguyen The Huu, Le Ba Phuong, Pham Thi Mai Huong, Tuyen Dinh Nguyen, *Formation of structural defects within Fe-UiO-66 for effective adsorption of arsenic from water*, International Journal of Environmental Science and Technology, 2022 (Q1, IF 3.519).

2. Nguyen Dinh Tuyen, Bui Van Vuong, Nguyen Thuong Tai, Pham Thai Hung, Nguyen Dinh Chung, Tran Quang Hung, Trinh Van Tuyen, Phan Do Hung, Do Thi Linh, **Nguyen Duc Hai**, Dinh Thi Ngo, *Synthesis of modified hierarchical titanium containing metal-organic framework materials meso-Ti@Zr-UiO-66 for arsenic removal from water*, Vietnam Journal of Chemistry, 2016, 6e2 54, 23-27.

3. **Nguyen Duc Hai**, Bui Van Vuong, Pham Thai Hung, Nguyen Dinh Chung, Tran Van Ha, Vu Minh Tan, Nguyen Dinh Tuyen, *synthesized metal organic frameworks materials (mof) for arsenate absorption in water,* Journal of Science and Technology, Hanoi University of Industry, 2017, 38, 90-93.

4. **Nguyen Duc Hai**, Vu Minh Tan, Dang Huu Canh, Nguyen Dinh Tuyen, *synthesis of metal organic frameworks materials containing ziconium with defections in frameworks,* Journal of Science and Technology, Hanoi University of Industry, 2018, 45, 86-89.5.

5. **Nguyen Duc Hai**, Vu Minh Tan, Nguyen The Huu, Nguyen Dinh Tuyen, *Synthesis of UiO-66 materials applied to arsenic adsorption in water*, Vietnam Journal of Catalysis and Adsorption, 2022, 11, 1, 22-28.